Practical Considerations in PSD Upper Bounding of Experimental Data

Mathieu Joerger and Sandeep Jada, *Virginia Tech,*

Steven Langel*, *The MITRE Corporation,*

Omar García Crespillo, *German Aerospace Center (DLR),*

Elisa Gallon, Boris Pervan, *Illinois Institute of Technology.*

ABSTRACT

In this paper, we develop a methodology to estimate the power spectrum of an experimentally-obtained data set for high-integrity modeling of Kalman filter (KF) input noise time correlation. In theory, power spectral density (PSD) upper-bounding can be used to determine time-correlated error models that guarantee bounds on the estimation error variance in recursive navigation algorithms such as KFs. This assumes that an empirical PSD is given. In practice, there is more than one way to determine a PSD from data. This PSD estimate depends on the number of samples in the data set, on the windowing process, and on the PSD frequency resolution. These parameters have an impact on the robustness of the PSD-upper-bounding model. In this paper, we analyze error model sensitivity to these parameters for example simulated random processes and for a one-year-long time-series of GPS orbit and clock ephemeris errors.

I. INTRODUCTION

This paper addresses three practical challenges encountered when determining a power spectral density (PSD) from time-correlated data for high-integrity Kalman filter (KF)-based navigation. In theory [1, 2], PSD-upper-bounding enables time-correlated measurement error modeling to upper-bound the estimation error variance of linear, recursive algorithms. In practice, empirical PSD determination depends on the number of samples in the data set, on the windowing process, and on the PSD frequency resolution. In this paper, we analyze the sensitivity of PSD-upper-bounding error models to these parameters for an example simulated random process and for a one-year-long time-series of GPS orbit and clock ephemeris errors.

Safety-critical navigation applications require that estimation errors be reliably quantified. Over the last two decades, significant effort was spent towards guaranteeing bounds on Global Navigation Satellite Systems (GNSS)-based position estimation errors in the context of satellite-based and ground-based augmentation systems (SBAS, GBAS) and Advanced Receiver Autonomous Integrity Monitoring (ARAIM) for aviation applications. Positioning error bounds were achieved by careful modeling of GNSS ranging measurement errors and by rigorous algorithm design that quantify integrity and continuity risks.

Emerging high-accuracy, high-integrity, and high-continuity navigation applications require the use of sequential estimators such as KFs. This poses new challenges for integrity monitoring because the time correlation of measurement errors must be robustly accounted for despite being uncertain. Bounding models for uncertain first-order Gauss Markov processes (FOGMP) are derived in the time and frequency domains in [3, 4] and are applied in GNSS/INS implementations in [5, 6]. The more general case of non-FOGMP stationary time-correlated processes is treated in references [1] and [2], which show that PSD upper bounding of independent measurement error sources guarantees an upper bound on KF estimation error variance. Using PSD upper bounding, finite-parameter models such as two-parameter FOGMP models can be use to safely account for complex random processes. However, there is no systematic approach to estimate an empirical PSD from experimental data to ensure high-integrity error modeling.

In response, in this paper, we develop a methodology to analyze the impacts of autocorrelation sequence (ACS) windowing parameters, estimated PSD frequency resolution, and data sample sparsity.

Section II is a problem statement further exposing the relevance of these three challenges for high-integrity PSD estimation using experimental data.

Section III addresses windowing parameters. In [1], a procedure is outlined for modeling correlated noise that involves applying

---

* The author's affiliation with The MITRE Corporation is provided for identification purposes only and is not intended to convey or imply MITRE's concurrence with, or support for, the positions, opinions, or viewpoints expressed by the author.

a rectangular or a tapered window to the ACS and then taking its Fourier transform to estimate the PSD. The window size can be limited by the maximum period over which a GNSS satellite is visible. Because rectangular windows cause spectral leakage in the Fourier transform, a tapered window with a roll-off period can be applied. In this paper, we analyze the impact of tapering on the PSD-bounding model of simulated random process. We observe that short-period tapering fails to reduce spectral leakage whereas longer-period tapering may incorporate unnecessary frequency content that would not impact realistic operations where a satellite's visibility period is limited. We outline a procedure for finding the window tapering period that minimizes the variance of the PSD-bounding process.

In Section IV, we address the fact that the PSD is estimated at discrete frequencies and the PSD is then upper-bounded at those frequencies for modeling. Ignoring that the PSD is a continuous function raises doubt as to whether the model's PSD truly exceeds the estimate at all frequencies because only a finite number of frequencies would be considered. In this paper, we develop a new automated method to account for the continuous nature of the PSD. It finds local PSD maxima using an analytical expression of the PSD. We give this expression in terms of a sum of sample-based coefficients multiplying cosine functions of integer multiples of the frequency. The maxima are then be upper-bounded for robust modeling. We evaluate this automated approach using samples drawn from a simulated random sample time series.

In Section V, we analyze the impact of sample size in PSD estimation. We use analytical expressions of FOGMP PSDs to illustrate the fact that, given a fixed GMP variance, a finite-sample time series has less low-frequency content than a continuous (infinite sample) time-process. This difference is quantified analytically and for an example simulated FOGMP.

Finally, Section VI implements the above procedures to derive a high-integrity model of time-correlated GPS satellite orbit and clock ephemeris errors.

II. PROBLEM STATEMENT: THREE CHALLENGES WITH PSD UPPER-BOUNDING

Assuming that a measurement error ACS is available, the method outlined in [1] and [2] uses the Wiener-Khinchin theorem to derive a PSD estimate. In the next paragraph, we will apply a window function to the ACS in Fig. 1a. A PSD-upper-bounding model $\bar{\mathcal{F}}(\Omega)$ can then be established as illustrated in Fig. 1b. For example, we may consider a FOGMP model because it is easily incorporated in a KF by state augmentation. Thus, for a linearly filtered measurement sequence with ACS shown in the left panel in Fig. 1, we can use the FOGMP model with PSD $\bar{\mathcal{F}}(\Omega)$ shown in the right panel to predict a guaranteed upper bound on the estimation error variance [1].
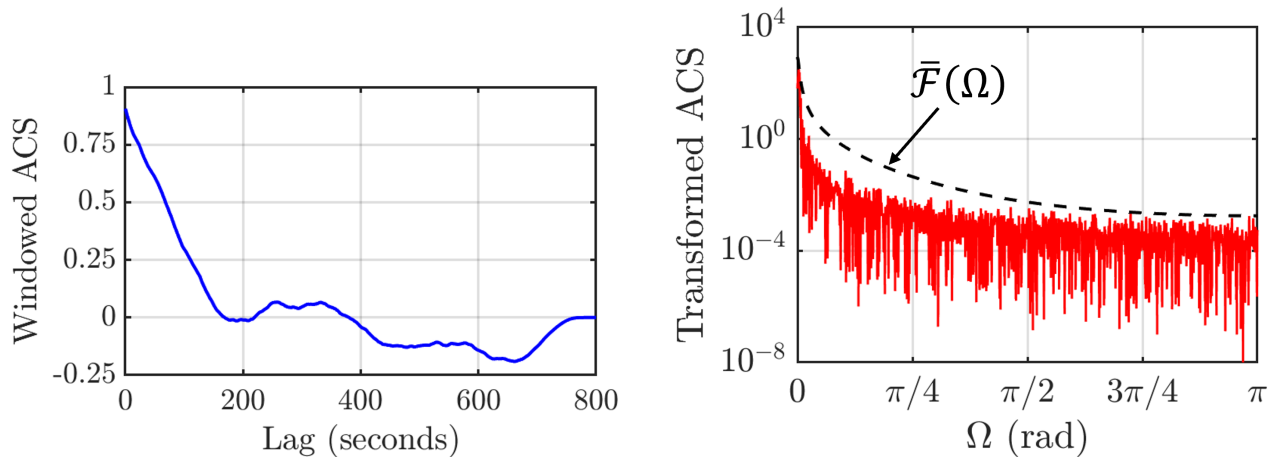
(a) Example time-correlated measurement noise autocorrelation sequence for a FOGMP evaluated at 1-second lag-intervals over 1400 samples and shown for lag times 0 to 800 s.

(b) Sample PSD of the measurement error process (in red) and PSD-upper-bounding FOGMP model (dashed black). The x-axis' circular frequency Ω is the frequency (in rad/s) multiplied by the sample interval Δt.

Figure 1: Overview of the PSD upper-bounding process.

Consider a KF measurement error process filtered over a time period not exceeding $n\Delta t$ where Δt is the sampling interval. For example, at a static GNSS receiver location, it is typical for satellite visibility periods to be such that $n\Delta t \leq 7$ hours. We assume that measurement noise components (e.g., satellite measurement errors) are mutually independent and that each measurement noise component is zero-mean and stationary over the interval. A conservative noise model is achieved when the noise model's PSD is such that [1]:

$$\bar{\mathcal{F}}(\Omega) \geq r_0 + 2 \sum_{l=1}^{n_w} \phi_l r_l \cos(l\Omega) \quad \text{for all } \Omega \in [0, \pi], \tag{1}$$

where $\bar{\mathcal{F}}(\Omega)$ is the time-correlated noise model PSD, r_l is the ACS of the noise component at lag index l corresponding to lag time $l\Delta t$ (shown on the left-hand-side panel in Fig. 1, and ϕ_l is the window function with $\phi_l = 1$ for $l \leq n$, $\phi_l = 0$ for $l \geq n_w$ and ϕ_l is defined in [3] as a monotonically decreasing function with values from 1 to 0 when l ranges from n to n_w.

In Eq. 1, we apply a windowing function ϕ_l because lag times longer than $n\Delta t$ are not encountered in operation. A rectangular ACS window over lag times 0 to $n\Delta t$ can achieve this goal. However, it causes spectral leakage with ringing effects that artificially distort the estimated PSD as shown in Fig. **??**. Such an estimate would cause the PSD upper-bound to be overly conservative. A tapered window is used instead with tapering parameter n_w illustrated in Fig. 2a. The sensitivity of model variance to n_w is analyzed in Section III.
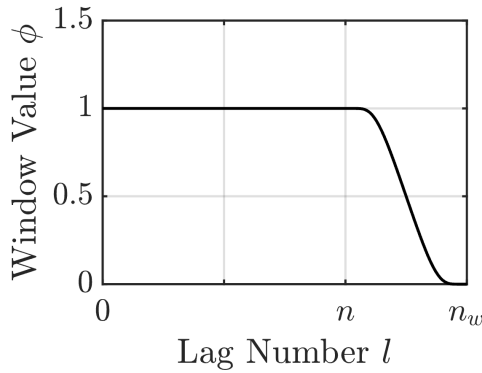
(a) Example tapered window with width n and tapering parameter n_w.
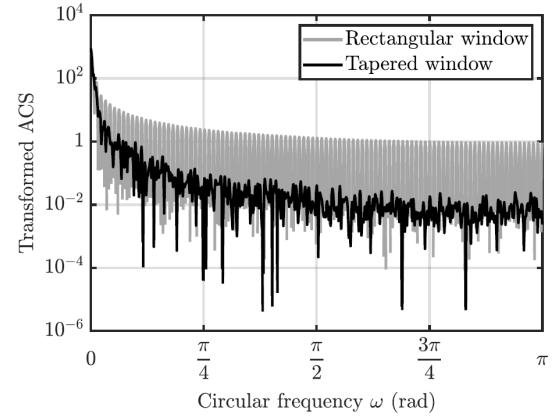
(b) Example PSD estimation using a rectangular window causing spectral leakage, and using a tapered window.

Figure 2: Overview of the ACS windowing process.

In addition, in Eq. 1, $\bar{\mathcal{F}}(\Omega)$ is a continuous function that must be bounding for all $\Omega \in [0, \pi]$. Typical numerical PSD estimation routines pick discrete values of Ω at regular frequency intervals. This approach does not guarantee that Eq. 1 is satisfied. We found practical cases, e.g., in inertial sensor data, where different frequency resolutions yielded significantly different results. Section IV presents a method to identify PSD peaks without PSD evaluation at arbitrary Ω-values.

Another practical consideration is that the estimated measurement error ACS $\hat{r}_l$ is derived from data, after verifying that the noise process is zero-mean and stationary [5]. The data set should be as large as possible to reduce ACS noisiness [7]. Sensitivity to the number of samples in the dataset is analyzed in Section II for a FOGMP.

III. PSD ESTIMATE SENSITIVITY TO WINDOWING

Two parameters define the windowing function ϕ_l in Eq. 1 as illustrated in Fig. 2. The window width n is determined by the operational filtering duration. In contrast, there is no obvious criterion to select the window tapering parameter n_w. Several values for n_w are evaluated in Appendices C and H of [7].

For the stationary noise process ACS in Fig. 1 with n=600, we can vary n_w-values to find the minimum variance FOGMP model that satisfies the PSD inequality in Eq. 1. Consider an FOGMP with time constant τ and variance σ^2. For now, PSD upper-bounds are found for each n_w-value using a time-consuming brute-force strategy: we vary FOGMP parameter values (σ and τ) till the empirical PSD is upper-bounded by the FOGMP model's PSD.

For each n_w-value, the minimum FOGMP variance value resulting from the two-dimensional search process is plotted in Fig. 3. The figure shows that the FOGMP variance reaches a minimum at a n_w-value highlighted by a vertical dashed black line. We observed this trend in all ACS that we analyzed. The reason is the following. To the left of dashed line, the PSD-bounding model variance decreases as spectral leakage decreases. To the right of dashed line, the model variance increases because frequency content is included in PSD estimation, which does not need to be modeled because ACF contributions beyond lag times $n\Delta t$ have no impact in actual operations. Thus, it is safe to consider the FOGMP model derived, in this example, for $n_w = 875$.
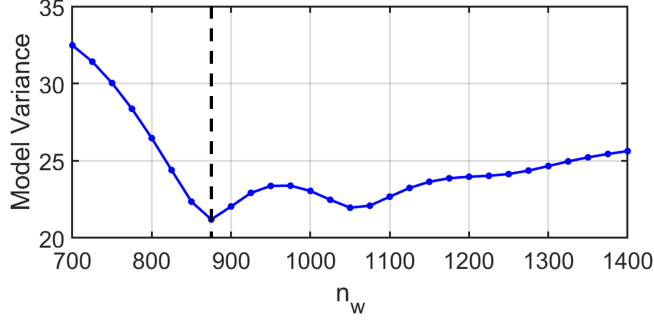
Figure 3: Example analysis of PSD-bounding model variance versus window tapering parameter n_w.

High-integrity error models are typically determined off-line using large amounts of historical data. It is therefore not essential to limit the model determination's computation time. Still, the curve in Fig. 3 took many hours to generate. Computation time reduction contributed to motivate the approach developed in Section IV where PSD peaks are analytically found instead of searching over many frequency values.

IV. EFFECTIVE FREQUENCY SAMPLING FOR PSD BOUNDING

This section develops an efficient method to determine a FOGMP model with PSD $\bar{\mathcal{F}}(\Omega)$ satisfying Eq. 1. For clarity of exposition, we fix the value of the FOGMP time constant τ and use the notation $\alpha = e^{(-\Delta t/\tau)}$. Clever ways to find α are described in [8]. Thus, we can formulate the problem of determining a variance-minimizing PSD-upper-bounding FOGMP model as follows:

$$
\begin{aligned}
&\text{minimize} \quad \sigma^2 \\
&\text{subject to} \quad \frac{(1-\alpha^2)\sigma^2}{1+\alpha^2-2\alpha\cos(\Omega)} \geq r_0 + 2\sum_{l=1}^{n_w} \phi_l r_l \cos(l\Omega) \\
&\text{for all} \quad \Omega \in [0, \pi].
\end{aligned}
\tag{2}
$$

This optimization problem must be considered for all values of $\Omega \in [0, \pi]$, which sets an infinite number of constraints that make Eq. 2 cumbersome to solve. Further, considering discrete Ω-values opens up the problem of adequate sampling of Ω. Figure 4 illustrates the fact that the empirical PSD's local peaks, and therefore the PSD upper bound, are sensitive to the sampling of Ω. The red and blue sample PSDs in Fig. 4 are respectively computed using a low and high Ω-resolution: the red PSD estimate fails to accurately capture the peaks showed on the blue curve. The right-hand-side panel is a zoomed in view of the PSD.
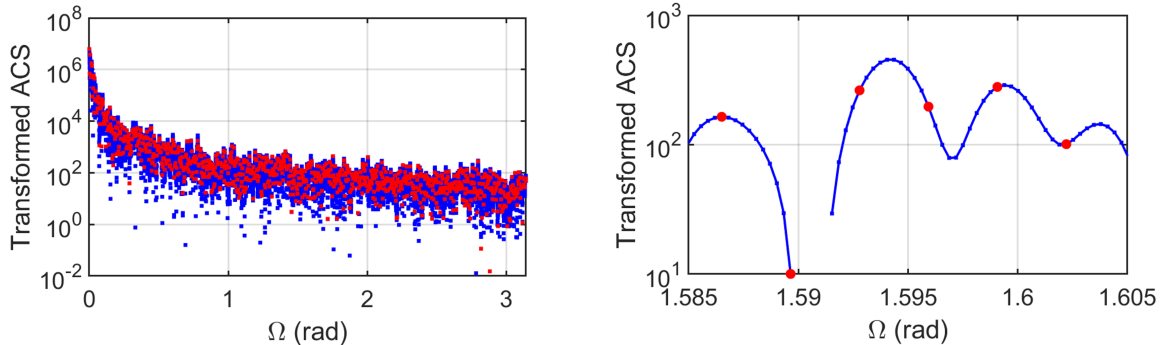

Figure 4: Example PSD Estimation for two different frequency resolutions of $10^{-4}\pi$ and $10^{-3}\pi$ respectively shown in blue and in red. The lower frequency resolution in red fails to accurately capture PSD peaks, which can result in underestimated PSD bounds and therefore optimisitic error models. (Windowing parameters in this example were $n = 600$ and $n_w = 720$)

In a forthcoming paper [8], we develop an analytic method to solve this problem not only for FOGMPs, but also for white noise

and second-order autoregressive models. A MATLAB implementation of the algorithm will be made publicly available.

Following this method, the FOGMP model variance is set to its minimum allowable value, i.e.:

$$\sigma^2 = \max_{\Omega} \left[\frac{1 + \alpha^2 - 2\alpha \cos(\Omega)}{(1 - \alpha^2)} \left(r_0 + 2 \sum_{l=1}^{n_w} \phi_l r_l \cos(l\Omega) \right) \right]. \tag{3}$$

Provided that the absolute maximum can be found, it can be shown that this absolute maximum must occur at $\Omega^* = 0$, $\Omega^* = \pi$, or $\Omega^* = \cos^{-1}(x^*)$, where x^* is a real root of the following generalized polynomial:

$$p(x) = \sum_{l=1}^{n_w} c_l U_l(x), \tag{4}$$

and where $U_l(x)$ is the lth order Chebyshev polynomial of the second kind. The values x^* can be efficiently found knowing that the roots of $p(x)$ are generalized eigenvalues of a pair of $n_w \times n_w$ matrices [9].

Thus, this analytical solution to Eq. 3 eliminates the need to reduce $\Omega \in [0, \pi]$ to a finite set. We implement this method on actual data in Section VI.

V. IMPACT OF NUMBER OF SAMPLES IN FOGMP PSD ESTIMATION

The theoretical PSD of a FOGMP with time constant τ and variance σ^2 can be written as [10]:

$$\mathcal{F}(\Omega) = \frac{\sigma^2(1 - \alpha^2)}{1 + \alpha^2 - 2\alpha \cos(\Omega)}. \tag{5}$$

Let N be the number of samples. Equation 5 can be interpreted as the FOGMP PSD obtained using a data set where N approaches infinity. The blue curve in Fig. 5 represents Eq. 5 evaluated for a FOGMP with $\Delta t / \tau = 0.01$ and variance $\sigma^2 = 1$ (both unit-less).
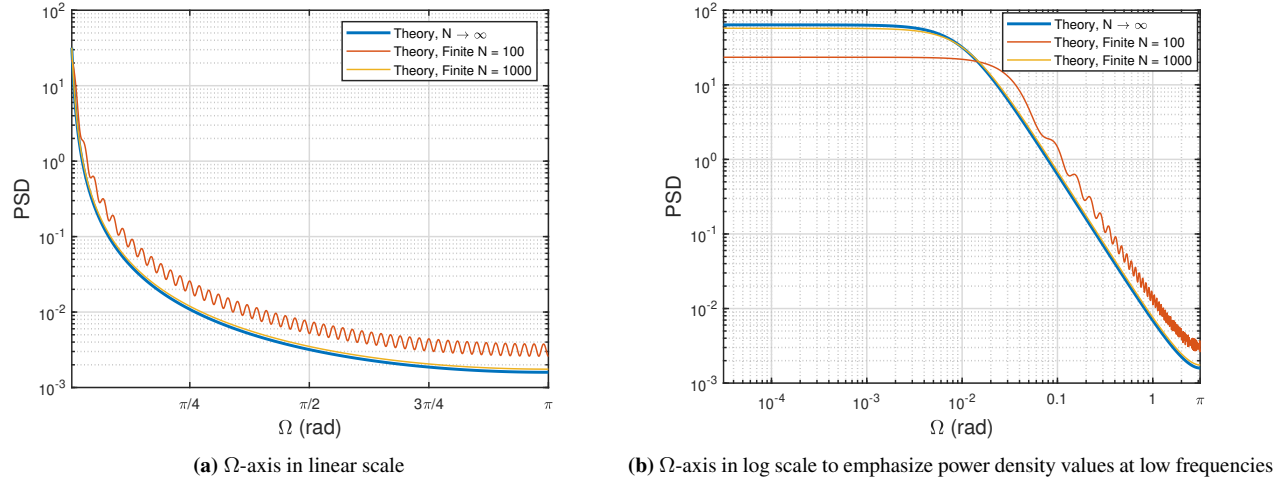

(a) Ω-axis in linear scale

(b) Ω-axis in log scale to emphasize power density values at low frequencies

Figure 5: Analytical FOGMP PSD curves for values of N ranging from 100 to approaching infinity.

In practice, N is finite. In Appendix, we derive a closed-form expression of a PSD estimate $\hat{\mathcal{F}}(\Omega)$ for a finite N. The derivation does not include an ACS-window with width $n \ll N$ as in Sections II to IV. Instead, the Appendix shows that deriving a PSD from a finite sample time series is equivalent to applying a triangular window to the ACS of the corresponding infinite sample time series. This triangular window does not eliminate spectral leakage as effectively as tapering in Fig. 2a, especially

for small values of N. However, the closed-form expression still provides key insights on the impact of N on PSD estimation. This expression can be written as:

$$\hat{\mathcal{F}}(\Omega) = 2\sigma^2 \, \text{Re} \left(\frac{N - (N+1)z_\Omega + z_\Omega^{N+1}}{N(1 - z_\Omega)^2} \right) - \sigma^2 \qquad \text{with} \quad z_\Omega \triangleq \alpha e^{(-i\Omega)}, \tag{6}$$

where Re( ) designates the real part of a complex number.

Figure 5 shows the theoretical FOGMP PSD derived using Eq. 6 for $N = 100$ and $N = 1000$. The figure's right-hand-side panel is the same as the left-hand-side but uses a log-scale Ω-axis to emphasize low frequency content. As expected, for a large value of N, the PSD approaches that of Eq. 5, whereas for a smaller value of N, we observe spectral leakage. Also expected is a knee in the curves located at $\Delta t/\tau = 0.01$. The lower N is, the weaker the low-frequency content becomes. The finite-N curves cross the 'infinite-N' curve because the area under all three curves must equal σ^2. For PSD-upper-bounding, we are concerned about underestimating the PSD, i.e., about the low-frequency content. A value of N can be determined to limit the low-frequency FOGMP PSD estimation error using the following expression derived from Eq. 5 and 6:

$$\hat{\mathcal{F}}(0) - \mathcal{F}(0) = \frac{2\sigma^2}{(1-\alpha)^2} \left(\frac{N - (N+1)\alpha + \alpha^{N+1}}{N} - 1 + \alpha \right). \tag{7}$$

VI. EXAMPLE IMPLEMENTATION FOR GPS SATELLITE ORBIT AND CLOCK EPHEMERIS ERRORS

In this section, we implement the automated time-correlated random process modeling method on actual data. Raw samples of GPS clock and orbit ephemeris errors for PRN 5 at 30 second intervals over Year 2018 are processed to obtain the PSD estimate in Fig. 6. Figure 6a shows the entire PSD, Fig. 6b zooms in on small Ω-values where the empirical PSD defines the FOGMP bound, i.e., where the red sample PSD curve touches the black-dashed FOGMP model curve.

It is worth noticing that this data was previously processed in [2] with intensive inputs from the authors, and the FOGMP that was then obtained matches the model from the automated process well. The new approach also considers all Ω-values, not only a discrete set of such values.

(a) Transformed ACS for all frequencies   **(b)** Zoomed-in view of the transformed ACS at low frequencies
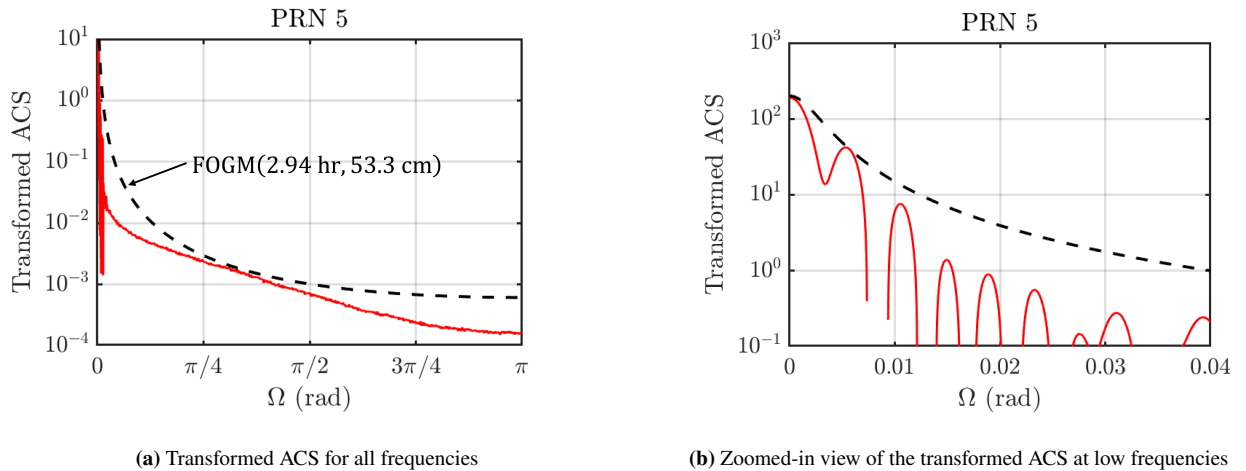
Figure 6: PSD (transformed ACS) of PRN 5 orbit and clock error over Year 2018 and associated FOGMP PSD upper-bound. (Windowing parameters were $n = 7$ hours and $n_w = 10$ hours.)

VII. CONCLUSION

In prior work, a theoretical criterion for defining correlated measurement noise models that guarantee a bound on the KF estimation error variance bound was derived. However, it left practical considerations on power spectral density (PSD) estimation unaddressed, including on the sensitivity of the empirical PSD estimate to the number of samples, on the impact of autocorrelation sequence (ACS) windowing, and on the fact that the PSD is a continuous function of frequency. An automated method was developed to find a minimum variance first-order Gauss Markov process (FOGMP) model, which was implemented to derive a robust model for GPS clock and orbit ephemeris error for PRN5 during Year 2018.

REFERENCES

[1] S. Langel, O. G. Crespillo, and M. Joerger, "A new approach for modeling correlated Gaussian errors using frequency domain overbounding," in *2020 IEEE/ION Position, Location and Navigation Symposium (PLANS)*. IEEE, 2020, pp. 868–876.

[2] E. Gallon, M. Joerger, and B. Pervan, "Robust modeling of GNSS orbit and clock error dynamics," *NAVIGATION: Journal of the Institute of Navigation*, vol. 69, no. 4, 2022.

[3] S. Langel, O. Garcia Crespillo, and M. Joerger, "Overbounding the effect of uncertain Gauss-Markov noise in Kalman filtering," *Navigation*, vol. 68, no. 2, pp. 259–276, 2021.

[4] O. G. Crespillo, S. Langel, and M. Joerger, "Tight bounds for uncertain time-correlated errors with Gauss-Markov structure in Kalman filtering," *IEEE Transactions on Aerospace and Electronic Systems*, 2023.

[5] O. Garcia Crespillo, "GNSS/INS Kalman filter integrity monitoring with uncertain time correlated error processes," Ph.D. dissertation, Ecole Polytechnique Federale de Lausanne, 2022.

[6] O. G. Crespillo, M. Joerger, and S. Langel, "Overbounding gnss/ins integration with uncertain gnss gauss-markov error parameters," in *2020 IEEE/ION Position, Location and Navigation Symposium (PLANS)*, 2020, pp. 481–489.

[7] E. Gallon, "High-integrity modeling of non-stationary kalman filter input error processes and application to aircraft navigation," Ph.D. dissertation, Illinois Institute of Technology, 2023.

[8] S. Langel, O. G. Crespillo, and M. Joerger, "Frequency-domain modeling of correlated gaussian noise in kalman filtering," *unpublished*.

[9] V. Noferini and J. Pérez, "Fiedler-comrade and fiedler–chebyshev pencils," *SIAM Journal on Matrix Analysis and Applications*, vol. 37, no. 4, pp. 1600–1624, 2016.

[10] C. Chatfield, *The analysis of time series: an introduction*, 6th ed. Florida, US: CRC Press, 2003.

A. FOGMP PSD ESTIMATE FROM FINITE NUMBER OF SAMPLES

This appendix aims at deriving an analytical expression of a PSD estimate $\hat{\mathcal{F}}(\Omega)$ for a finite number of samples N. This is performed in two steps. First, we show that in general, deriving a PSD from a finite time series is equivalent to applying a triangular window to the ACS of the corresponding infinite time series. Then, we use the Wiener Khinchin theorem to estimate the PSD of an FOGMP from a triangular-windowed ACS.

1. The PSD of a finite discrete time series is the DTFT of the triangular-windowed infinite time series' ACS

In order to express $\hat{\mathcal{F}}(\Omega)$ in terms of N, we derive a PSD estimate as a mean periodogram itself derived from measurement error sample time series ν_n, for $n = 0, ..., N-1$. The discrete-time Fourier Transform (DTFT) of a finite sample time series extracted from an infinite time series using a rectangular window function $\phi_{\text{R},n}$ is expressed as:

$$f(\Omega) = \sum_{n=-\infty}^{\infty} \nu_n \phi_{\text{R},n} e^{-i\Omega n} \quad \text{where} \quad \phi_{\text{R},n} = \begin{cases} 1 & n \in [0, N-1] \\ 0 & \text{otherwise} \end{cases} \tag{8}$$

The periodogram of this windowed sample time series is defined as:

$$p(\Omega) = \left(\sum_{n=-\infty}^{\infty} \nu_n \phi_{\text{R},n} e^{-i\Omega n} \right) \left(\sum_{n=-\infty}^{\infty} \nu_n \phi_{\text{R},n} e^{i\Omega n} \right)$$

Using the fact that the DTFT of ν_{-n} is $f(-\Omega)$, we can re-write this equation as:

$$p(\Omega) = \left(\sum_{n=-\infty}^{\infty} \nu_n \phi_n e^{-i\Omega n} \right) \left(\sum_{n=-\infty}^{\infty} \nu_{-n} \phi_{-n} e^{-i\Omega n} \right) \tag{9}$$

This product of DTFTs can be expressed as the DTFT of a discrete-time convolution. The discrete-time convolution of two function $h(l)$ and $g(l)$ is: $(h * g)[n] = \sum_{l=-\infty}^{\infty} h[l]g[n-l]$. Substituting $h(l) = \nu_l \phi_{\text{R},l}$ and $g(n-l) = \nu_{l-n} \phi_{\text{R},l-n}$, we can

rewrite Eq. 9 as:

$$p(\Omega) = \sum_{n=-\infty}^{\infty} \left(\sum_{l=-\infty}^{\infty} (\nu_l \phi_{\mathrm{R},l})(\nu_{l-n} \phi_{\mathrm{R},l-n}) \right) e^{-i\Omega n}$$

$$= \sum_{n=-\infty}^{\infty} \left(\sum_{l=-\infty}^{\infty} (\phi_{\mathrm{R},l-n} \phi_{\mathrm{R},l})(\nu_{l-n} \nu_l) \right) e^{-i\Omega n}$$

Let $E[\ ]$ be the expected value operator. The expectation of the periodogram scaled by $1/N$ is the PSD estimate $\hat{\mathcal{F}}(\Omega)$. Using the definition of the ACS r_n $(r_n = E[\nu_{l-n} \nu_l])$, we obtain the following expression:

$$\hat{\mathcal{F}}(\Omega) = \frac{1}{N} \sum_{n=-\infty}^{\infty} \left(\sum_{l=-\infty}^{\infty} (\phi_{\mathrm{R},l-n} \phi_{\mathrm{R},l}) \right) r_n e^{-i\Omega n} \tag{10}$$

The windowing function under the double-sum can be interpreted as a convolution of rectangular windows, i.e., a triangular window function $\phi_{\mathrm{T},n}$, which can be expressed as:

$$\phi_{\mathrm{T},n} = \frac{1}{N} \sum_{l=-\infty}^{\infty} (\phi_{\mathrm{R},l-n} \phi_{\mathrm{R},l}) = \frac{1}{N} \begin{cases} N - |n| & n \in [-N+1, N-1] \\ 0 & \text{otherwise} \end{cases} \tag{11}$$

Equation 10 becomes:

$$\hat{\mathcal{F}}(\Omega) = \frac{1}{N} \sum_{n=-(N-1)}^{(N-1)} (N - |n|) r_n e^{-i\Omega n} \tag{12}$$

2. Finite-sample FOGMP PSD estimate

For a FOGMP, Eq. 12 becomes:

$$\hat{\mathcal{F}}(\Omega) = \sigma^2 \sum_{n=-N+1}^{N-1} \left(1 - \frac{|n|}{N} \right) \alpha^{|n|} e^{(-i\Omega n)} \tag{13}$$

Splitting the sum at zero and rearranging the summation indices, we can rewrite Eq. 13 as:

$$\hat{\mathcal{F}}(\Omega) = \sigma^2 \left[\sum_{n=0}^{N-1} \left(1 - \frac{n}{N} \right) \overline{z}_\Omega^n + \sum_{n=0}^{N-1} \left(1 - \frac{n}{N} \right) z_\Omega^n - 1 \right] \quad \text{where} \quad z_\Omega \triangleq \alpha e^{(-i\Omega)} \tag{14}$$

and where $\overline{z}_\Omega$ is the complex conjugate of z_Ω. The term '-1' is added to avoid accounting for the '$n = 0$' terms twice. The sum of complex conjugates can be rewritten as:

$$\hat{\mathcal{F}}(\Omega) = \sigma^2 \left(2 \operatorname{Re} \left(\sum_{n=0}^{N-1} \left(1 - \frac{n}{N} \right) z_\Omega^n \right) - 1 \right) \tag{15}$$

Using geometric series formulas and simplifying, we get the following closed-form expression:

$$\hat{\mathcal{F}}(\Omega) = \sigma^2 \left[2 \operatorname{Re} \left(\frac{N - (N+1)z_\Omega + z_\Omega^{N+1}}{N(1 - z_\Omega)^2} \right) - 1 \right] \tag{16}$$